Absence of lattice strain anomalies at the electronic topological transition in zinc at high pressure

Gerd Steinle-Neumann* and Lars Stixrude
Department of Geological Sciences, University of Michigan, Ann Arbor, Michigan 48109-1063

Ronald E. Cohen
Geophysical Laboratory and Center for High Pressure Research, Washington, DC 20015-1305
and Seismological Laboratory, California Institution of Technology, Pasadena, California 91125
(Received 15 May 2000; published 3 January 2001)

High-pressure structural distortions of the hexagonal close-packed (hcp) element zinc have been a subject of controversy. Earlier experimental results and theory showed a large anomaly in lattice strain with compression in zinc at about 10 GPa which was explained theoretically by a change in Fermi surface topology. Later hydrostatic experiments showed no such anomaly, resulting in a discrepancy between theory and experiment. We have computed the compression and lattice strain of hcp zinc over a wide range of compressions using the linearized augmented plane-wave method paying special attention to *k*-point convergence. We find that the behavior of the lattice strain is strongly dependent on *k*-point sampling, and with large *k*-point sets the previously computed anomaly in lattice parameters under compression disappears, in agreement with recent experiments.

DOI: 10.1103/PhysRevB.63.054103 PACS number(s): 61.66.Bi, 71.15.Nc, 71.20.−b, 64.30.+t

I. INTRODUCTION

Zinc and cadmium are unique among the hexagonal close-packed (hcp) transition metals in that the axial ratio ($c/a = 1.856$ for zinc and 1.886 for cadmium) is far from the ideal value defined by hard-sphere packing ($c/a = \sqrt{8/3} = 1.633$). Upon compression, the axial ratio decreases towards the ideal value. Lynch and Drickamer[1] observed that the decrease in c/a with increasing pressure was not smooth; subsequent experiments yielded inconsistent results on the nature of this anomaly.[2–7] Takemura confirmed the anomaly using a methanol-ethanol-water mixture[4,7] (MEWM) as a pressure medium in diamond-anvil cell experiments: he observed the *a* axis expanding over a small range of compression, yielding a rapid decrease of the axial ratio c/a. *Ab initio* computations found similar behavior[8–10] and provided an explanation for the anomaly by means of changes in the Fermi surface topology under compression.[9,11] Takemura recently repeated his experiments but using helium as pressure medium[12] which is more nearly hydrostatic than MEWM, but found that both axes compressed monotonically with no anomaly in c/a, contrary to his earlier experiments and theory.

The most recent experimental results call previous theoretical studies[8–10] into question. All previous theoretical studies show the anomaly in the axial ratio whether the local-density approximation (LDA) (Refs. 8 and 9) or the generalized gradient approximation (GGA) (Ref. 10) to the exchange correlation potential is used. The anomaly has been connected to changes in the electronic structure:[9,11] Fast *et al.*[9] observe one electronic topological transition (ETT) at the high-symmetry point *K* on the Brillouin-zone boundary forming an ellipsoidal piece (needle) in the Fermi surface. Novikov *et al.*[11] see at least one additional ETT at approximately the same compression, also at *K*, where disconnected pieces form a three-leg structure of the Fermi surface along the *K*-*M* directions upon compression. Depending on c/a with compression Novikov *et al.*[11] propose one more ETT at *L* (butterfly) reconciling previous contradictory results from first principles calculations.[13] All previous computations were performed with typical Brillouin-zone sampling (no more than 1000 *k* points in the irreducible wedge of the Brillouin zone).

In an attempt to understand the discrepancy of the hydrostatic experiments[12] and previous computational results[9,10] we calculate the equation of state, lattice constants, and electronic structure of zinc over a wide compression range from first principles paying particular attention to the convergence of the calculations with respect to reciprocal-space integration. In Sec. II we introduce the method used and elaborate the computational details of our first-principles calculations. Section III focuses on our results for the equation of state, lattice constants, and electronic structure. We compare our results to experiments at ambient conditions and high pressure and to previous theoretical work. Discussion and conclusions follow.

II. METHOD

We investigate the energetics of hcp zinc using the full-potential linearized augmented plane-wave method (LAPW) (Ref. 14) with GGA.[15] Core states are treated self-consistently using the full Dirac equation for the spherical part of the potential, while valence states are treated in a semirelativistic approximation neglecting spin-orbit coupling. $3s$, $3p$, $3d$, $4s$, and $4p$ states are treated as valence electrons. The muffin-tin radius R_{MT} is 2.0 Bohr over the whole compression range considered.

We perform calculations at three sets of Brillouin-zone sampling, $24\times24\times24$, $32\times32\times32$, and $48\times48\times48$ special *k* points,[16] yielding 732, 1632, and 5208 *k* points in the irreducible wedge of the Brillouin zone for the hcp lattice, respectively. The lowest *k*-point sampling is comparable to the previous GGA study[10] while the latter two are much denser

than any previously published results. The size of the basis is set by $R_{MT}K_{max}=9.0$, where K_{max} is the largest reciprocal-space vector. We use Fermi broadening with an electronic temperature of 5 mRy. For the densest *k*-point mesh we also perform calculations without electronic broadening for a selected subset of volumes and do not see any significant change in our results: equilibrium axial ratios remain within ± 0.005, the uncertainty of our results.

We carry out total-energy calculations over a wide range of unit-cell volumes. At each volume we perform calculations for several different values of the axial ratio and find the equilibrium structure by fitting the results to a quadratic. The equation of state is obtained by describing the energy-volume curve with a third-order expansion in Eulerian finite strain.[17] We consider unit-cell volumes ranging from 60 to 110 Bohr^3 for $24\times24\times24$ *k* points and focus on the range in which the anomaly in c/a occurs (90–102.5 Bohr^3) for $32\times32\times32$ and $48\times48\times48$ *k*-point meshes.

III. RESULTS

A. Equation of state

A comparison of the pressure-volume relation between our results and static experiments[7,12] (Fig. 1 and Table I) shows good agreement at low pressure. At higher pressure theory differs significantly from the results of the MEWM diamond-anvil cell experiments;[7] this is consistent with previous theoretical results.[10]

To investigate whether nonhydrostaticity may be responsible for the discrepancy we also compare to the results of shock wave experiments[18] where hydrostaticity is readily achieved[19] (Fig. 1 and Table I). The Hugoniot is reduced to a 0-K isotherm by solving the Rankin-Hugoniot equation.[20] We estimate the thermal pressure ($P_{th}=\gamma E_{th}/V$) along the Hugoniot, with γ the Grüneisen parameter and E_{th} the thermal energy. We approximate the thermal energy by the Dulong Petit law ($C_V^{lat}=3R$); the electronic contribution to the thermal pressure is negligible (the temperature along the Hugoniot is less than 2000 K). We assume the Grüneisen parameter is proportional to compression ($\gamma=\gamma_0 V/V_0$) with γ_0 its zero pressure value evaluated from the thermodynamic definition ($\gamma=\alpha K_T/C_V\rho$), where the thermal expansivity α, the isothermal bulk modulus K_T, specific heat C_V, and density ρ at zero pressure are taken from the literature.[21]

The reduced Hugoniot agrees with our GGA results much better than the static experiments; differences in volume are less than 1.5%. The large discrepancy between the static and shock wave experiments indicates that the MEWM experiments[7] may be biased by nonhydrostaticity.

B. Lattice constants

Total energy as a function of axial ratio for the $24\times24\times24$ *k*-point mesh shows an unusually large scatter about the quadratic fit in c/a (Fig. 2). With increasing number of *k* points the scatter decreases and the minimum becomes better defined. In contrast to the previous GGA results[10] we do not see multiple minima in c/a for any volume and find the axial ratio reliably resolved to within ± 0.005, within the symbol size in Fig. 1. The curvature of energy as a function of c/a varies considerably for the different *k*-point meshes, showing that elastic constants will also be strongly dependent on *k*-point sampling, as the shear elastic constant (C_S) is related to this strain.[22]

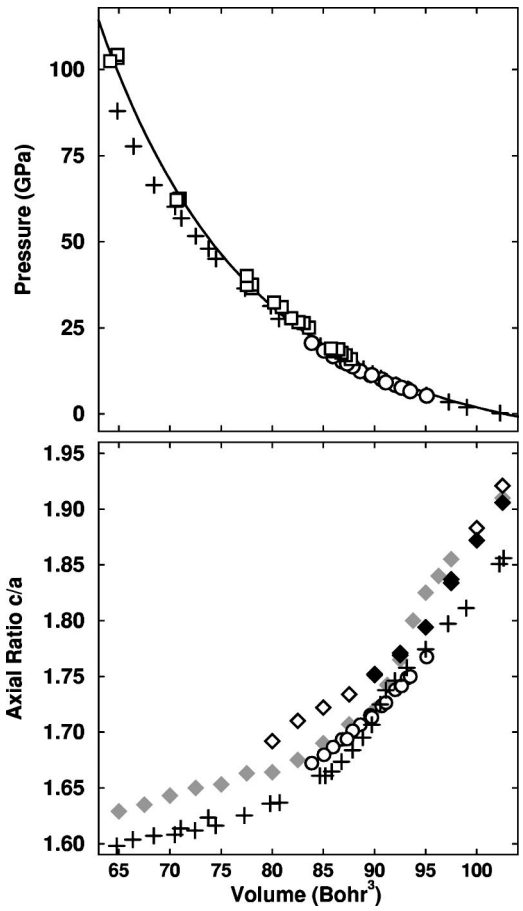

FIG. 1. Axial ratio c/a and equation of state for zinc from our calculations and experiment. The lower panel compares our results for c/a (gray diamonds $24\times24\times24$ *k* points, open diamonds $32\times32\times32$ *k* points, and filled diamonds $48\times48\times48$ *k* points) to static experiments using methanol ethanol water mixture (Ref. 7, pluses) and helium (Ref. 12, circles). The equation of state for zinc is shown in the upper panel for our calculations (line) and the same two set of diamond-anvil cell experiments (same symbols as above). The open squares show shock wave experiments (Ref. 18) reduced to a 0-K isotherm.

The development of the axial ratio c/a with compression differs for the three sets of computations considerably (Fig. 1). For $24\times24\times24$ *k* points we see an anomaly similar to that in the MEWM experiments:[4,7] after an initial linear decrease in the axial ratio (102.5–95 Bohr^3) the slope in c/a steepens (95–90 Bohr^3) before decreasing again at higher pressures. The dependence of c/a on compression for *k*-point meshes of $32\times32\times32$ and $48\times48\times48$ is much smoother; the anomaly in c/a has disappeared. The difference between experiment and theory is less than 4% in c/a which is typical of all electron calculations.[23] At higher compression ($V<70$ Bohr^3) the theoretical value smoothly approaches 1.61; the MEWM experiments converge to 1.59.

TABLE I. Equation of state parameters for our calculations (GGA) and experiment: V_0, K_0, and K_0' are the equilibrium volume, bulk modulus, and its pressure derivative at V_0, respectively. Due to the restricted compression range of the calculations with higher k-point sampling ($32\times32\times32$ and $48\times48\times48$) and for the static experiments with helium as a pressure medium, we constrain K_0' and V_0.

Method	V_0 [Bohr^3]	K_0 [GPa]	K_0'
GGA $k=24$	102.8	64	5.2
GGA $k=32$		64	
GGA $k=48$		63	
Equilibrium properties	102.6[21]	60[33]	
Reduced Hugoniot (Ref. 18)		69	4.9
Experiment MEWM (Ref. 7)		65	4.7
Experiment He (Ref. 12)		61	
Experiment N (Ref. 5)		63	5.2
FP-LMTO (GGA) (Ref. 10)	101.5	60	

The nature of the anomaly is revealed by considering the lattice constants separately (Fig. 3). The c axis compresses monotonically with decreasing volume in all computations and experiments considered. Theory overpredicts c by less than 2%, and there is little difference in c for the two denser k-point meshes. An expansion of the a axis for the $24\times24\times24$ k-point calculations and the MEWM experiments cause the anomaly in c/a (Fig. 3). For the two denser k-point meshes a compresses monotonically; for volumes smaller than $V=95$ Bohr^3 a follows a linear trend with the same slope as the helium experiments. For volumes greater than $V=95$ Bohr^3, a is less compressible than it is at higher pressure. For the larger k-point samplings the calculations underestimate a by less than 1%, while with $24\times24\times24$ k-point the maximum difference is approximately 1.5%.

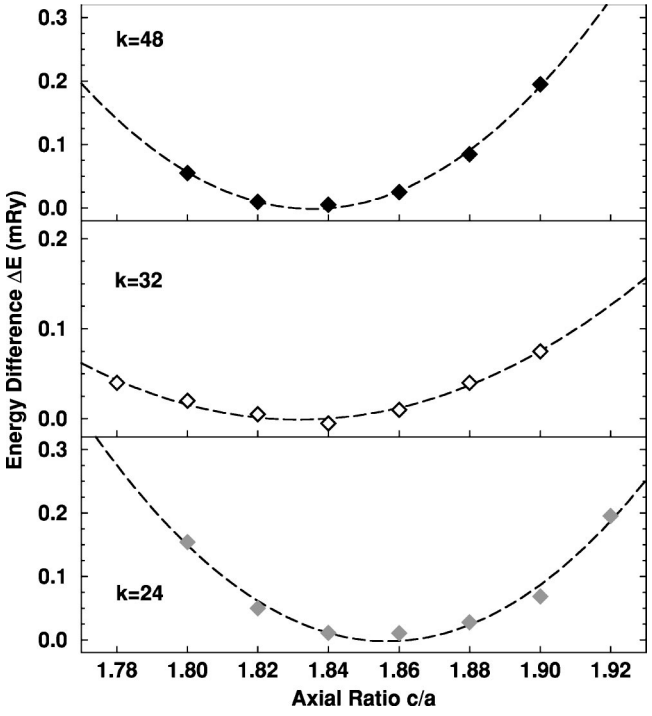

FIG. 2. Relative energies as a function of the axial ratio c/a for $V=97.5$ Bohr^3. The lower, middle, and upper panel shows results for $24\times24\times24$, $32\times32\times32$, and $48\times48\times48$ k points, respectively. The lines show quadratic fits in c/a to the results.

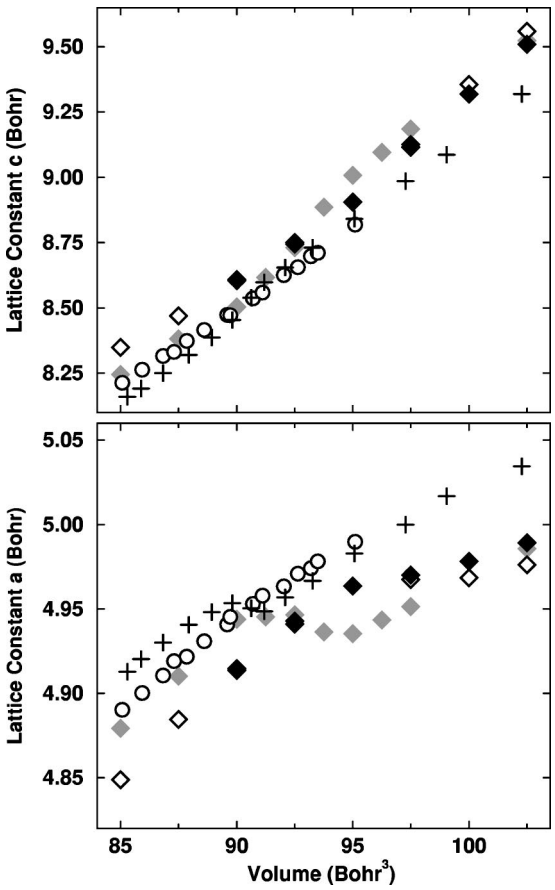

FIG. 3. Compression of the two axes a and c in the hexagonal cell for zinc over the compression range $V/V_0=0.80-1.0$. In the upper panel we compare our results (diamonds) for c (gray $24\times24\times24$, open $32\times32\times32$, and filled $48\times48\times48$ k points) with the static experiments by Takemura using methanol-ethanol-water mixture (pluses, Ref. 7) and helium (open circles, Ref. 12) as a pressure medium. For a in the lower panel the same symbols are used. Note the approximately fivefold difference in range of axes compressibilities for c and a.

To illustrate this point further we evaluate the linear compressibility for the two axes $k_x=-(1/x)(\partial x/\partial P)$ (with $x=a,c$) for our results and the static experiments[7,12] using central differences (Fig. 4). Our results for $24\times24\times24$ k points show an anomaly in k_a similar in character and magnitude to that found in the MEWM experiments. For denser k-point sampling the anomaly in k_a is shifted towards lower pressure and its magnitude decreases with increasing number of k points. For k_c an anomaly exists as well for both the MEWM experiments[7] and the calculations with the smallest k-point mesh, it is, however, less pronounced than for k_a and is absent from the results for the two denser k-point meshes.

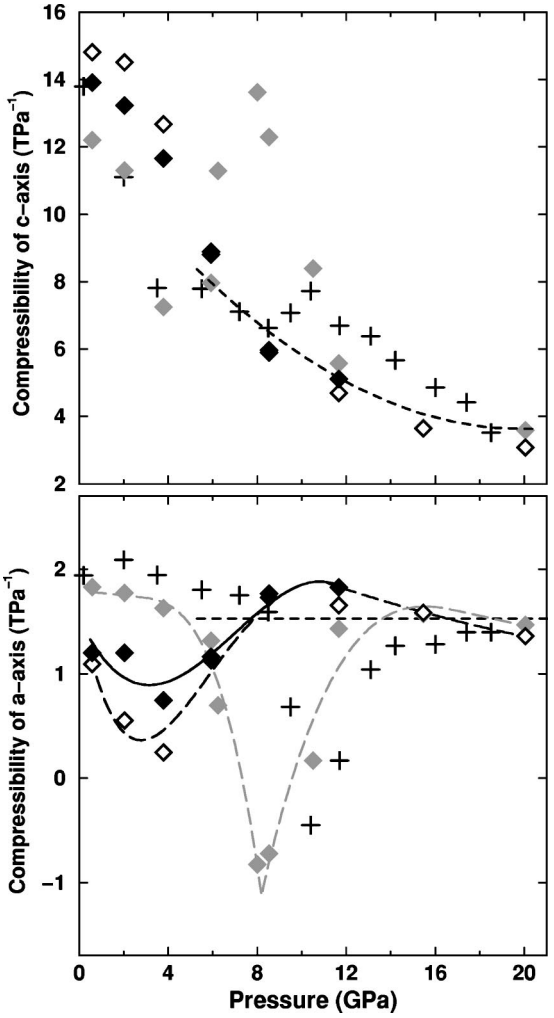

FIG. 4. Compressibility of the two axes k_a and k_c for our results (k-point sampling $24\times24\times24$ with grey diamonds, for $32\times32\times32$ and $48\times48\times48$ we use a fit to the results in the long dashed and solid line, respectively) and static experiments using a methanol-ethanol-water mixture (pluses, Ref. 7) and helium (average in dashed line, Ref. 12) as a pressure pressure medium.

C. Electronic structure

The band structure of zinc under compression changes considerably from $V=102.5$ Bohr^3 to $V=95$ Bohr^3 (Fig. 5). The electronic structure is in excellent agreement with the previous GGA results.[10] The major change in band structure occurs at the high-symmetry point K on the Brillouin-zone boundary where three bands [K_7,K_8,K_9 (Ref. 24)] cross the Fermi energy under compression, changing the topology of the Fermi surface. From the band structure we see the needle around K and also the connection of the three-leg piece at K. Focusing on the development of the band structure at K we consider the eigenvalues of the K_7, K_8, and K_9 states (Fig. 6). For the $24\times24\times24$ k-point calculations these bands show a quadratic volume dependence and cross the Fermi energy at $V=97.5$ Bohr^3 (K_7 and K_8) and $V=97$ Bohr^3 (K_9). For the two denser k-point meshes the eigenvalues depend linearly on volume and the crossing points are indistinguishable for $32\times32\times32$ and $48\times48\times48$ k points. The

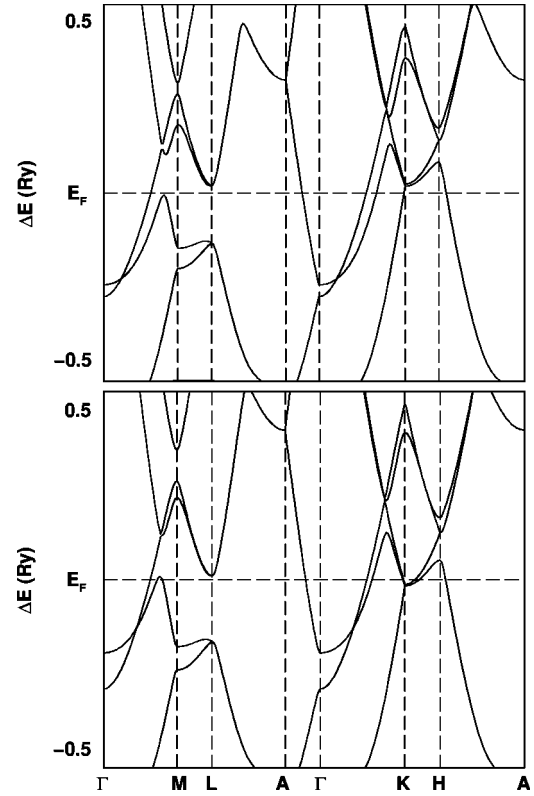

FIG. 5. Band structure for zinc along high-symmetry directions in the first Brillouin zone around the Fermi energy. The upper panel shows the band structure at zero pressure ($V=102.5$ Bohr^3), the lower panel at $V=95$ Bohr^3 at their equilibrium c/a (1.91 and 1.79, respectively).

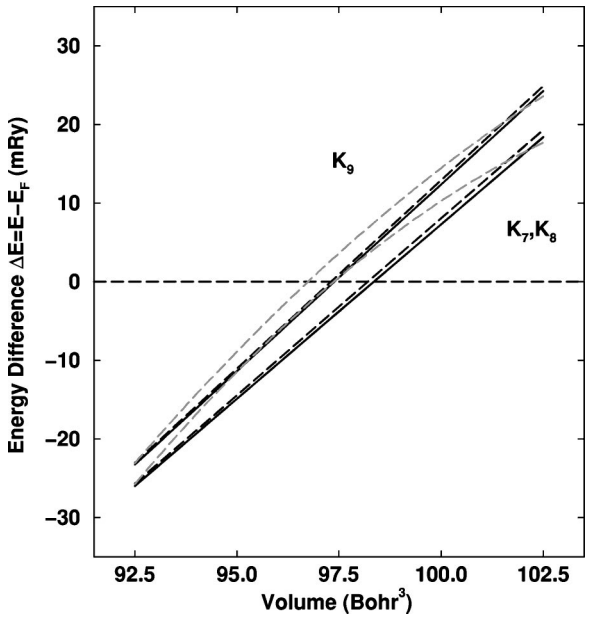

FIG. 6. Energy differences of the bands to the Fermi energy at the high-symmetry point K on the first Brillouin-zone boundary as a function of unit-cell volume. Gray dashed, dashed, and solid lines are results for k-point sampling of $24\times24\times24$, $32\times32\times32$, and $48\times48\times48$, respectively.

crossings occur at slightly higher volume than for the 24 $\times 24 \times 24$ *k*-point mesh ($V=98$ and 97.5 Bohr^3 for K_7, K_8, and K_9, respectively), but the difference is small compared with the effect of *k*-point sampling on the lattice parameters.

IV. DISCUSSION

The ETT discussed in the last section has previously been invoked as an explanation for the anomaly in *a*-axis compressibilities.[9,11] In contrast to these studies we find that the occurrence of the ETT is independent of the calculated anomaly in *a*-axis compressibility, as the location of abnormal compression of *a* shifts with increasing *k*-point sampling towards higher volumes (Figs. 3 and 4) while the ETT always occurs at approximately the same volume (Fig. 6). The anomaly in *a*-axis compression seen in previous calculations appears to be a consequence of insufficient *k*-point sampling. The results presented here for *a* (Fig. 3) and linear compressibility k_a (Fig. 4) suggest that even for the densest *k*-point mesh we use ($48\times48\times48$) the lattice parameters are not converged.

The discrepancy between the MEWM and helium experiments can be attributed to freezing of the MEWM pressure medium which is known to occur at about 10 GPa.[25] Freezing substantially increases the nonhydrostatic component of stress as recognized previously in high-pressure experiments on forsterite (Mg_2SiO_4).[26] At room temperature helium also freezes within the pressure range of the experiment (11.5 GPa),[27] but remains soft enough to maintain hydrostaticity.[26] Recent neutron inelastic-scattering experiments under compression[28,29] show no softening or anomaly in the phonon frequency, supporting the monotonic compression of both axes as seen in our dense *k*-point calculations and the helium experiments.

In retrospect it occurs as a fortuitous (or unfortunate) coincidence that for *typical* computational parameters comparable behavior in linear compressibilities is found in first-principles electronic structure calculations and for experiments with nonhydrostatic conditions, despite the fundamentally different underlying physical problem. Following the same notion the observation of anomalies in the axial ratio under compression for cadmium in experiments[7] and theory using both LDA (Ref. 30) and GGA (Ref. 10) may also be an artifact due to nonhydrostatic conditions in the experiments and insufficient convergence with respect to computational parameters as well.

The ETT, however, might have important effects on higher-order physical properties such as elasticity. For tantalum a similar change in electronic structure as for zinc has been found under compression which has little effect on the equation of state[31] but appears in the elastic constants.[32]

V. CONCLUSIONS

Using the first-principles LAPW method with GGA we calculate the equation of state, structural parameters, and electronic structure of zinc over a wide compression range. We perform calculations for three different *k*-point samplings of the first Brillouin zone ($24\times24\times24$, $32\times32\times32$, and $48\times48\times48$ *k* points) and find lattice parameters, in particular the *a* axis, strongly dependent on the number of *k* points, while little or no effect can be seen on the equation of state and band structure. For lattice constants we find that a previously observed anomaly in *a*-axis compressibility shifts to lower pressure and decreases in amplitude as we increase *k*-point sampling from $24\times24\times24$ to $48\times48\times48$. This anomaly is not coupled to a change in electronic band structure as has been proposed before; we observe the ETT occurring at approximately the same volume for all sets of computational parameters.

The disappearance of the anomaly in lattice constants for our results is in agreement with recent static experiments using helium as a pressure medium. The remaining anomaly in *a*-axis compressibility indicates that structural parameters are not fully converged even for the prohibitively large *k*-point sampling we perform.

ACKNOWLEDGMENTS

We greatly appreciate helpful discussion with W. Holzapfel and K. Takemura at different stages of this project and thank H. Krakauer and D. Singh for use of their LAPW code. This work was supported by the National Science Foundation under Grant Nos. EAR-9614790 and EAR-9980553 (L.S.), and in part by DOE ASCI/ASAP Subcontract No. B341492 to Caltech DOE W-7405-ENG-48 (R.E.C.). Computations were performed on the SGI Origin 2000 at the Department of Geological Sciences at the University of Michigan and the Cray SV1 at the Geophysical Laboratory, support by NSF Grant No. EAR-9975753 and by the W. M. Keck Foundation.

*Electronic address: gerd@umich.edu

[1] R.W. Lynch and H.G. Drickamer, J. Phys. Chem. Solids **26**, 63 (1965).
[2] D.B. McWhan, J. Appl. Phys. **36**, 664 (1965).
[3] O. Schulte, A. Nikolaenko, and W.B. Holzapfel, High Press. Res. **6**, 169 (1991).
[4] K. Takemura, Phys. Rev. Lett. **75**, 1807 (1995).
[5] O. Schulte and W.B. Holzapfel, Phys. Rev. B **53**, 569 (1996).
[6] J.G. Morgan, R.B. VonDreele, P. Wochner, and S.M. Shapiro, Phys. Rev. B **54**, 812 (1996).
[7] K. Takemura, Phys. Rev. B **56**, 5170 (1997).
[8] S. Meenakshi, V. Vijayakumar, B.K. Godwal, and S.K. Sikka, Phys. Rev. B **46**, 14 359 (1992).
[9] L. Fast, R. Ahuja, L. Nordström, J.M. Wills, B. Johansson, and O. Eriksson, Phys. Rev. Lett. **79**, 2301 (1997).
[10] D.L. Novikov, A.J. Freeman, N.E. Christensen, A. Svane, and C.O. Rodriguez, Phys. Rev. B **56**, 7206 (1997).
[11] D.L. Novikov, M.I. Katsnelson, A.V. Trefilov, A.J. Freeman, N.E. Christensen, A. Svane, and C.O. Rodriguez, Phys. Rev. B **59**, 4557 (1999).
[12] K. Takemura, Phys. Rev. B **60**, 6171 (1999).
[13] M. Steiner, W. Potzel, H. Karzel, W. Schiessl, M. Köfferlein, and

G.M. Calvius, J. Phys.: Condens. Matter **8**, 3581 (1996).
[14] D. J. Singh, *Planewaves, Pseudopotentials and the LAPW Method* (Kluwer, Norwell, 1994).
[15] J. Perdew, K. Burke, and M. Ernzhofer, Phys. Rev. Lett. **77**, 3865 (1996).
[16] H.J. Monkhorst and J.D. Pack, Phys. Rev. B **13**, 5188 (1976).
[17] F. Birch, J. Geophys. Res. **95**, 227 (1952).
[18] S. P. Marsh, *LASL Shock Hugoniot Data* (University of California Press, Berkeley, 1980).
[19] J.M. Brown and R.G. McQueen, J. Geophys. Res. **91**, 7485 (1986).
[20] V. N. Zharkov and V. A. Kalinin, *Equations of State for Solids at High Pressure and Temperature* (Consultant Bureau, New York, 1971).
[21] A. James and M. Lord, *Index of Chemical and Physical Data* (Van Nostrand Reinhold, New York, 1992).
[22] G. Steinle-Neumann, L. Stixrude, and R.E. Cohen, Phys. Rev. B **60**, 791 (1999).
[23] L. Fast, J.M. Wills, B. Johansson, and O. Eriksson, Phys. Rev. B **51**, 17 431 (1995).
[24] R.W. Stark and L.M. Falicov, Phys. Rev. Lett. **19**, 795 (1967).
[25] G.J. Piermarini, S. Block, and J.D. Barnett, J. Appl. Crystallogr. **44**, 5377 (1973).
[26] R.T. Downs, C.S. Zhan, T.S. Duffy, and L.W. Finger, Am. Mineral. **81**, 51 (1996).
[27] J.M. Besson and J.P. Pinceaux, Science **206**, 1073 (1979).
[28] S. Klotz, M. Braden, and J.M. Besson, Phys. Rev. Lett. **81**, 1239 (1998).
[29] A.W. Overhauser, Phys. Rev. Lett. **81**, 4022 (1998).
[30] B.K. Godwal, S. Meenakshi, and R.S. Rao, Phys. Rev. B **56**, 14 871 (1997).
[31] R.E. Cohen, O. Gülseren, and R.J. Hemley, Am. Mineral. **85**, 338 (2000).
[32] O. Gülseren, R.E. Cohen, and H. Krakauer, Bull. Am. Phys. Soc. **44**, 1490 (1999).
[33] H. R. Schober and H. Dederichs, in *Elastic, Piezoelectric, Piezooptic, Electrooptic Constants, and Nonlinear Dielectric Susceptibilities of Crystals*, edited by K.-H. Hellwege and A. W. Hellwege, Landolt-Börnstein, New Series III, Vol. 11, Pt. 3 (Springer, Berlin, 1979).